Quantitative electron tomography : the effect of the three-dimensional point spread function

Reference:

Heidari Mezerji Hamed, van den Broek Wouter, Bals Sara.- *Quantitative electron tomography : the effect of the three-dimensional point spread function*

Ultramicroscopy - ISSN 0304-3991 - 135(2013), p. 1-5

DOI: http://dx.doi.org/doi:10.1016/j.ultramic.2013.06.005

Handle: http://hdl.handle.net/10067/1113970151162165141

Quantitative electron tomography: the effect of the three-dimensional point spread function

Hamed Heidari Mezerji[a], Wouter Van den Broek[b], Sara Bals[a]

[a] *EMAT, University of Antwerp, Groenenborgerlaan 171 B-2020 Antwerp*
[b] *Institut für Experimentelle Physik, Universität Ulm, Albert-Einstein-Allee 11, 89081 Ulm, Germany*

Abstract

The intensity levels in a three-dimensional (3D) reconstruction, obtained by electron tomography, can be influenced by several experimental imperfections. Such artifacts will hamper a quantitative interpretation of the results. In this paper, we will correct for artificial intensity variations by determining the 3D point spread function (PSF) of a tomographic reconstruction based on high angle annular dark field transmission electron microscopy. The large tails of the PSF cause an underestimation of the intensity of smaller particles, which in turn hampers an accurate radius estimate. Here, the error introduced by the PSF is quantified and corrected a posteriori.

Keywords: Radius Distribution, Electron Tomography, Artifact Correction

1. Introduction

In recent years, new developments in the field of materials science and nanotechnology have been driving the demand for quantitative characterization at the nanoscale. In many studies, the distribution of the diameter of nanoparticles or nanostructures in general is of importance. Transmission electron microscopy (TEM) is an excellent technique to study nanomaterials, but one should never forget that these images correspond to a two-dimensional (2D) projection of a three-dimensional (3D) object. Therefore, electron tomography for inorganic materials has been developed and applied in an increasing number of investigations over the last 15 years [1, 2, 3, 4].

When performing an electron tomography experiment, the specimen is tilted over an angular range as large as possible. Acquisition of the same area of interest is made every few degrees, typically every 1 or 2 degrees. Once a tilt series of images is obtained, the series is aligned and used as an input for a mathematical algorithm that reconstructs the 3D structure. Despite the progress that has been made concerning novel tomography holders [5], acquisition schemes and reconstruction algorithms [6, 7, 8], quantitative electron tomography is still not straightforward.

Accurate quantification of the particle diameter, requires a segmentation step following the reconstruction. Unfortunately, automatic segmentation by, for example, thresholding is hampered by artifacts that may be present in the reconstruction [9]. As a result, segmentation is mostly carried out manually.

In order to overcome this problem, it is important to eliminate reconstruction artifacts as much as possible. The most important artifact is due to the fact that a specimen holder can often not be tilted over the full angular range because of the limited spacing in between the pole pieces of the objective lens. In addition, the thickness of a sample, the TEM grid or the holder can lead to shadowing at higher tilt angles. This results in missing information, which is referred to as the missing wedge [10]. Nowadays, the missing wedge can be avoided using on-axis tilt tomography, but this technique can not be applied for all nanomaterials. The most apparent artifact due to the missing wedge is an elongation of the resolution along the beam direction [2]. Also other factors will lead to artifacts, for example misalignment and a limited number of projection images.

Recently, Ref.[11] has reported that the reconstructions of smaller particles show a lower intensity than reconstructions of particles of the same composition with a larger radius. In Sec.2, the origin of this artifact and its effect on segmentation and radius estimation is shown. Furthermore, a strategy to correct the radius estimates is proposed. In Sec.3 experiments illustrating our assertions are presented. In Sec.4 the results of these experiments are discussed.

2. Theory and Calculation

The imaging system for an electron tomography experiment consists of three basic steps: acquisition of the 2D projection images, alignment of the projection images and finally the 3D reconstruction. Imperfections during each step introduce blurring in the final result, which in this paper is described as a convolution with the $\mathrm{PSF_{3D}}$, the 3D point spread function. Previous investigations [12] have shown that an experimental reconstruction with the simultaneous iterative reconstruction technique (SIRT) is space-invariant to a good approximation.

For electron tomography, it is required that the intensity in each 2D projection image can be regarded as a monotonic function of the projection of the physical quantity to be reconstructed [13, 14]. In materials science, high angle annular dark field scanning transmission electron microscopy (HAADF-STEM) [15] is one of the imaging techniques that fulfill this projection requirement. Using this technique, the detector gathers electrons that are incoherently scattered to high angles (> 50 mrad) with respect to the electron beam direction. Ideally, the image intensity scales with a projection along the beam direction of the atomic number of the specimen raised to a power of about 1.7 [16, 17, 18]. Reconstructed particles of a specific composition, e.g. Au, are expected to yield a single gray value for the whole reconstruction.

To determine the $\mathrm{PSF_{3D}}$, we follow the approach as proposed in [12], where intensity profiles are extracted at the edge of a reconstructed nanoparticle along principal axes x, y and z (shown in figure 1). For an ideal reconstruction, such intensity profile is expected to be a step function. In practice, however, the

profile is smoothened. In this paper, the profiles are fitted to an edge spread function (ESF) [12],

$$ESF(x) = \frac{a_1}{1 + \exp\left(\frac{-(r-x)}{\sigma}\right)} + \frac{a_2}{1 + \exp\left(\frac{r-x}{\sigma}\right)}, \tag{1}$$

where r is the edge position, σ is the width of the edge, a_1 is the intensity in the particle and a_2 is the intensity of the particle's surrounding medium, as illustrated in Figure 2. The ESF in Eq. (1) is a sum of two logistic distributions[19]. The heavy tails of the logistic distribution, as compared to a normal distribution, often increase the robustness of the analysis. That is why the function has been proposed in earlier studies [20] to approximate the distribution of unknown variables. Since two logistic functions add up to a new logistic function superposed on a constant background, the one-dimensional PSF, $\mathrm{PSF_{1D}}$, can be obtained by deriving the logistic function with respect to x and a renormalization to 1. The result reads as:

$$PSF_{1D} = \frac{\exp(\frac{-x}{\sigma})}{\sigma(1 + \exp(\frac{-x}{\sigma}))^2} \tag{2}$$

To extend the $\mathrm{PSF_{1D}}$ in three dimensions, the widths σ_x, σ_y and σ_z are measured along each of the principle axes and combined as,

$$t^2 = \frac{x^2}{\sigma_x^2} + \frac{y^2}{\sigma_y^2} + \frac{z^2}{\sigma_z^2}, \tag{3}$$

yielding the $\mathrm{PSF_{3D}}$:

$$\mathrm{PSF_{3D}} = \frac{\exp(-t)}{(1 + \exp(-t))^2} \frac{1}{N}, \tag{4}$$

with N a normalization factor.

The large tails of the $\mathrm{PSF_{3D}}$ spread out the intensity of a reconstructed particle, and since the particle's total intensity must be conserved, the intensity in the center reduces. This effect is expected to be more severe for smaller particles than for larger particles and to become negligible if the particles are much broader than the $\mathrm{PSF_{3D}}$. The solid line in Figure 3 shows the expected gray value in the particle center as a function of diameter, note how the intensity levels off for larger particles.

This intensity variation also affects the result of segmentation through thresholding. In a simulation, a set of particles is convolved with the $\mathrm{PSF_{3D}}$. Then a thresholding is applied, where the threshold is set to half the intensity of the center of a very large particle. Afterwards, the diameters of the segmented particles are measured. Figure 4 shows the dependence between both. Note how the $\mathrm{PSF_{3D}}$ places a lower bound on the detectable particle diameters: in this example, a particle with a true diameter that approaches zero, yields a measured diameter of about 4.4 nm. Eventually, the true diameters are retrieved by applying this function to the measured diameters, thus correcting the effect of the finite $\mathrm{PSF_{3D}}$. The solid curve in Figure 4 is therefore called the correction function in the remainder of this paper. The correction function returns the true diameter of the particle based on the measured value from the experiment.

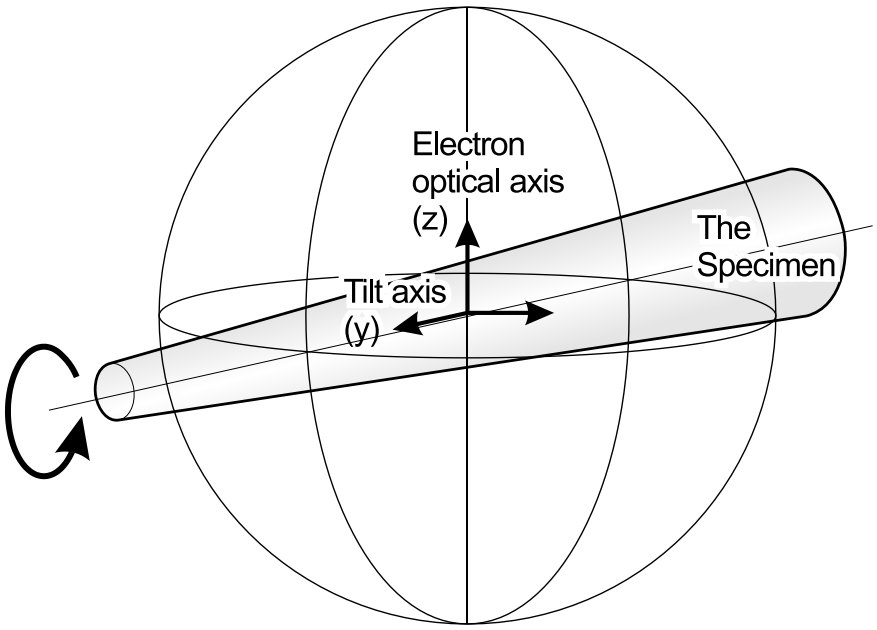

Figure 1: Schematic drawing of the geometry of a single tilt axis tomography experiment of a pillar-shaped specimen. The principle tomography axes are shown.

3. Materials and Methods

A micropillar specimen is prepared using focused ion beam (FIB) milling. The sample contains Pb nanoparticles distributed in a Si matrix [21]. Using a Fischione 2050 dedicated on-axis tomography holder, a tilt series is recorded using a Jeol 3000F operated at 300 kV. The acquisition is performed by focusing the 2D projections using the z-height control of the microscope stage. A tilt series of 2D projection images is acquired over an angular range of (-90 °, +90 °) and using an angular increment of 2 °. The alignment procedure for the series is performed using an iterative cross-correlation in FEI Inspect3D [22]. The reconstruction based on 20 iterations of SIRT [12] is performed using FEI inspect 3D. A voltex (volume) rendering of the reconstruction is presented in figure 5.

4. Results and Discussions

The point spread function has also been investigated for experiments in which a missing wedge is present [12]. Here, we aim to investigate the effect of the point spread function on quantification of electron tomography results in which a missing wedge is absent. The effect of the missing wedge when quantifying results from an electron tomography experiment has been the subject of earlier studies [9]. It was shown that it is far from straightforward to obtain

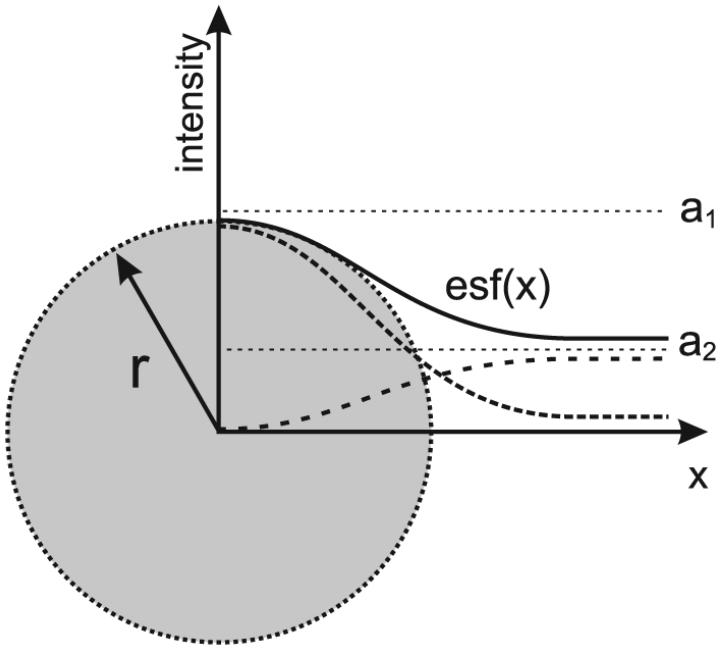

Figure 2: A schematic drawing showing the analytical model of the ESF. The intensity profile acquired from the reconstruction of the particle is modeled as a function of distance, using two combined sigmoid curves. Parameters a_1 and a_2 correspond to the intensities inside and outside the particle, respectively and the grey disk represents the particle.

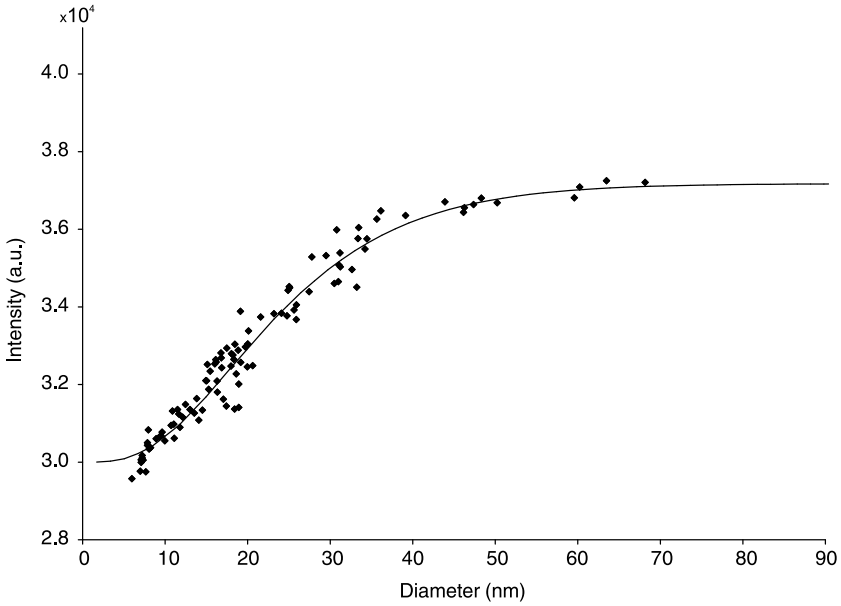

Figure 3: The intensity in the center of the Pb particles as a function of particle diameter. The solid curve gives the simulation and the points the experiments.

any quantitative results in 3D in case a reconstruction is obtained by applying a conventional reconstruction algorithm (e.g. SIRT) to an incomplete tilt series.

4.1. The attenuation of intensity

We assumed that the attenuation of intensity caused by $\mathrm{PSF_{3D}}$ results in the phenomenon that is observed in [23]. Therefore we tried to simulate the attenuation of intensity for the series of Pb particles. The $\mathrm{PSF_{3D}}$ of the reconstruction is measured according to the procedure explained in section 2. The intensity profiles are extracted normal to the surface of the particles parallel to the main tomography axes from 8 particles of various sizes according to [12]. These profiles are chosen symmetrically around the edge onset of the particles with five pixels on either side. The corresponding σ values (according to equation 1) are listed in Table 1. The mean values for σ are 2.1, 1.6 and 2.0 nm for σ_x, σ_y and σ_z respectively. Since the measurements do not suffer from a missing wedge, the x-axis and the z-axis are equivalent and σ_x and σ_z are thus expected to be equal.

Next, simulated spherical particles of varying diameters are convolved with the $\mathrm{PSF_{3D}}$. The particle diameters cover the range of the experimental measurements. For each convolution the intensity in the center of the particle is measured. This procedure is summarized in the flow chart presented in figure 6. In figure 3, the solid line represents the measured intensity at the center

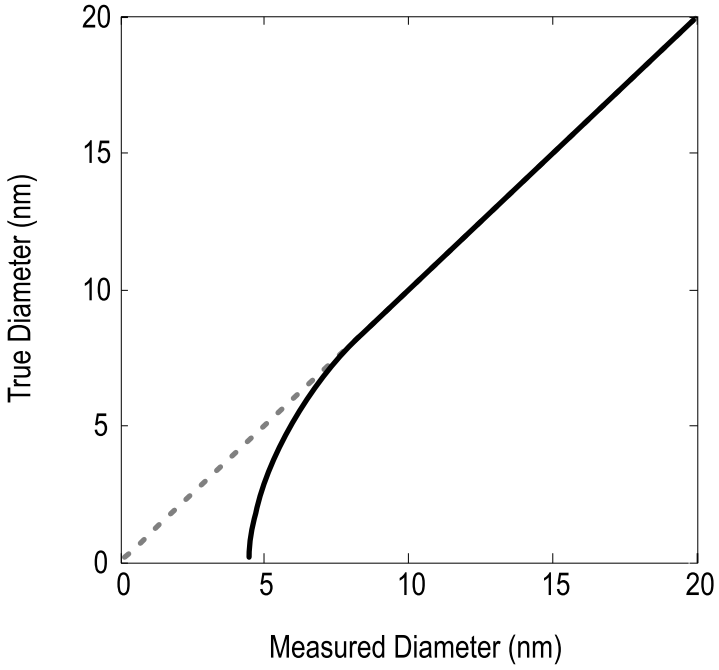

Figure 4: The solid curve shows the relation between the real particle diameter and the diameter obtained from segmentation. The deviation from the ideal case (dashed curve) is caused by the convolution with the PSF_{3D} and places a lower bound of 4.4 nm on the estimation of the diameter. The solid curve is used to correct the measured diameters and is denoted as the correction function in this paper.

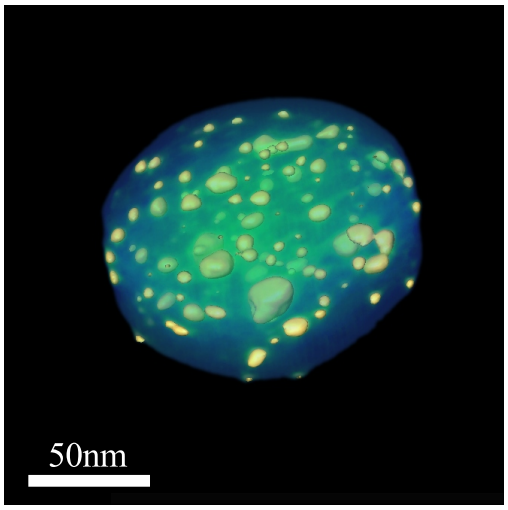

Figure 5: Volume rendering of the reconstructed Pb nanoparticles dispersed in Si matrix. The series is acquired over a tilt range of $\pm 90\,^{\circ}$.

Particle diameter (nm)	σ_x (nm)	σ_y (nm)	σ_z (nm)
27.5	2.0	1.7	2.2
18.2	2.1	1.5	2.1
17.5	2.0	1.6	1.9
15.7	2.2	1.5	2.0
14.2	1.9	1.6	1.9
13.9	2.1	1.6	2.0
12.3	2.1	1.4	2.1
11.9	2.1	1.7	2.1

Table 1: The σ values extracted along main tomography axes. These values are measured from the reconstructed Pb particles varying in diameter. The mean values along directions x,y, and z are 2.1 1.6 and 2.0 respectively. These values are used in the equations 3, 4 to calculate the PSF of the system.

of nanoparticles showing that the simulations are in accordance with the experimental intensities at the center of the reconstructed Pb-particles. These measurements indeed, confirm the findings of Ref.[23]. The simulation result in Fig. 3 is fitted to the experiments with a linear transformation to correct any rescaling that has occurred during the acquisition and the reconstruction of the data. Furthermore, it is observed that the intensity at the center of the nanoparticles saturates for larger particle diameters, in our experiment around 40 nm.

4.2. The correction of particle diameter measurements

To investigate the effect of PSF_{3D} on the estimate of particle diameters, a set of particles is convolved with the PSF_{3D} in a simulation. Next, in order to segment the particles, a thresholding is applied to the resulting convolution, where the threshold is set to half the intensity of the center of a very large particle (saturated intensity in figure 3). Figure 4 shows the measured diameter after segmentation (solid curve) and the true diameter of the particles (dashed line). The solid curve referred to as the correction function in section 2 can be used to correct the measured diameters. It also indicates how PSF_{3D} places a lower bound on the detectable particle diameter. A particle with a true diameter that approaches zero, yields a measured diameter of 4.4 nm.

Therefore it can be deduced that all segmented particles with a measured diameter of below the lower bound must be non-physical and result artificially from the segmentation procedure. Therefore, they can be safely omitted from the histogram. The correction function is then applied to the remaining measured diameters, thereby yielding the true diameters. In figure 7 the histograms before and after diameter correction are presented. Assuming a log-normal diameter distribution [24, 25, 26], the geometric mean before and after correction is 12.3 and 11.3 nm and the geometric standard deviation before and after correction is 1.7 and 2.1. This results in a 95% confidence interval of

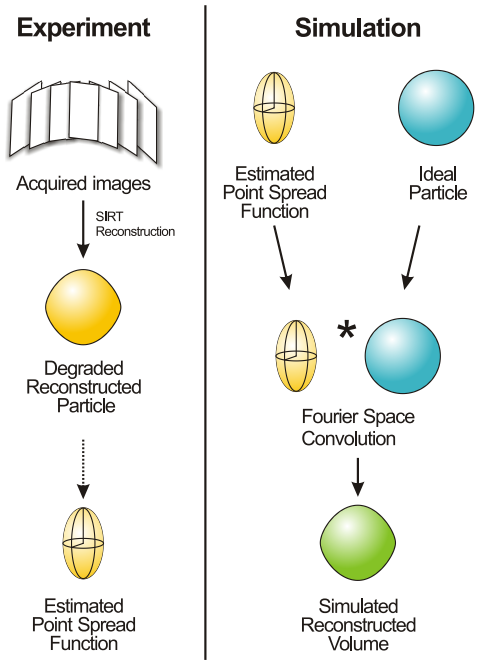

Figure 6: A diagram showing how the measurements are performed. Three one-dimensional PSF are measured and then a simulated PSF_{3D} is calculated. The resulting PSF_{3D} is convolved with simulated particles of varying diameters after which the intensity at the center of the particle is measured.

(4.1 nm, 37.0 nm) for the uncorrected distribution and (2.6 nm, 50.1 nm) for the corrected distribution.

5. Summary

In this work we explain how the three-dimensional point spread function affects the intensity of reconstructed particles as a function of their diameter. It was then shown how this artificial intensity variation impedes proper image segmentation which results in an inaccurate estimation of the diameter. The theoretical predictions were corroborated with experimental reconstructions of Pb-particles. Eventually, a correction of the measured diameters was performed. This showed that without correction, the geometrical mean of the diameter distribution in our experiments was overestimated and that the width of the distribution was severely underestimated. This approach can be considered as an optimized route to 3D quantitative information.

6. Acknowledgements

The authors acknowledge financial support from the European Union under the Seventh Framework Program under a contract for an Integrated Infrastructure Initiative. Reference No. 312483-ESTEEM2. S. Bals and H. Heidari Mezerji are grateful to the fund for Scientific Research Flanders. W. Van den Broek acknowledges the German Research Foundation (grant nr. KO 2911/7-1). Authors also thank M. Van Bael for provision of the samples and E. Biermans for the acquisition of a tilt series.

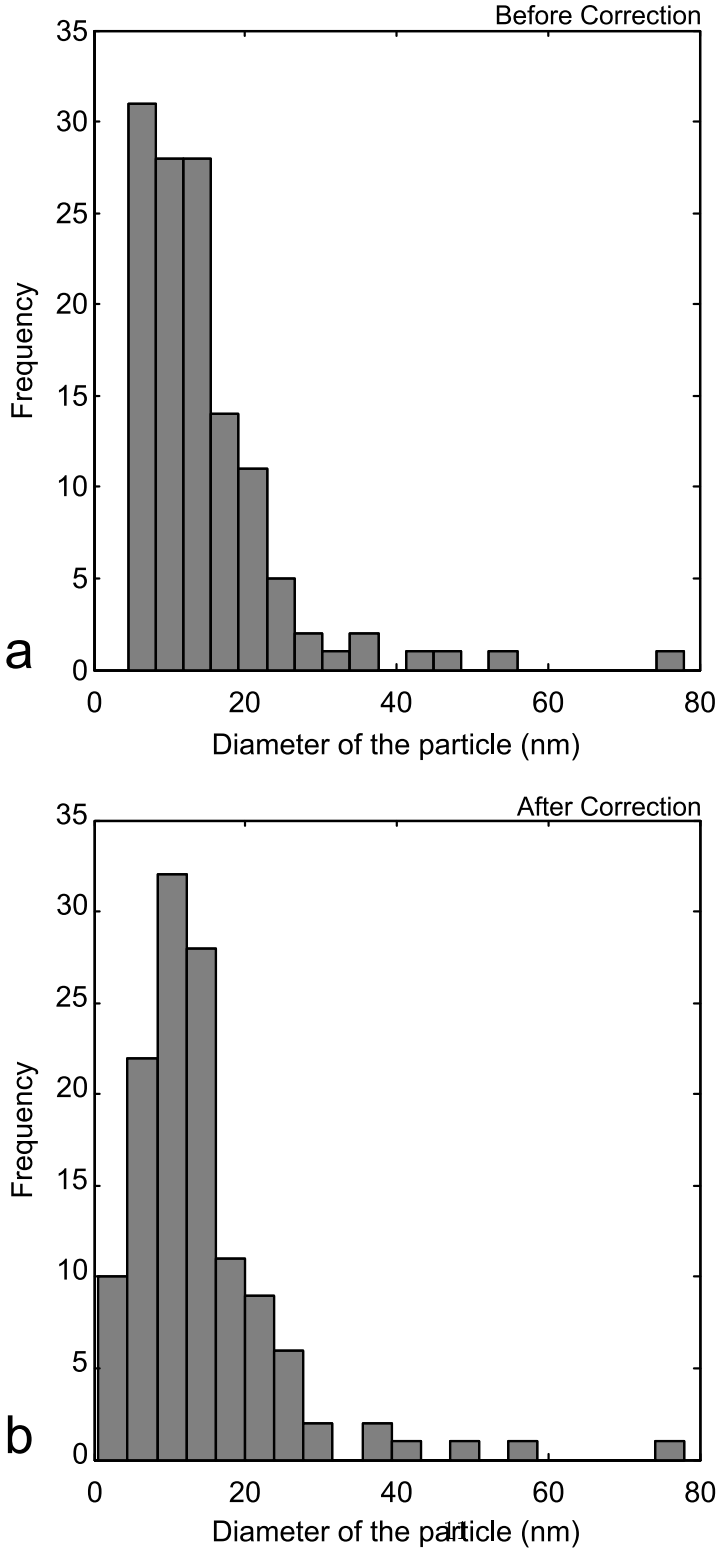

Figure 7: Particle diameter distributions from a set of reconstructed Pb nanoparticles, (a) segmented using a single graylevel as a threshold and (b) after the correction scheme explained in section 4.

References

[1] U. Ziese, C. Kubel, A.J. Verkleij, and A.J. Koster. Three-dimensional localization of ultrasmall immuno-gold labels by haadf-stem tomography. *Journal of Structural Biology*, 138(1-2):58–62, 2002.

[2] P.A. Midgley and M. Weyland. 3d electron microscopy in the physical sciences: the development of z-contrast and eftem tomography. *Ultramicroscopy*, 96(3-4):413–431, 2003.

[3] Paul A. Midgley and Rafal E. Dunin-Borkowski. Electron tomography and holography in materials science. *Nat Mater*, 8(4):271–280, April 2009.

[4] Bart Goris, Sara Bals, Wouter Van den Broek, Enrique Carbó-Argibay, Sergio Gómez-Graña, Luis M. Liz-Marzán, and Gustaaf Van Tendeloo. Atomic-scale determination of surface facets in gold nanorods. *Nat Mater*, 11(11):930–935, November 2012.

[5] N. Kawase, M. Kato, H. Nishioka, and H. Jinnai. Transmission electron microtomography without the "missing wedge" for quantitative structural analysis. *Ultramicroscopy*, 107(1):8–15, 2007.

[6] W. Van den Broek, S. Van Aert, and D. Van Dyck. A model based atomic resolution tomographic algorithm. *Ultramicroscopy*, 109:1485–1490, 2009.

[7] W. Van den Broek, A. Rosenauer, B. Goris, G.T. Martinez, S. Bals, S. Van Aert, and D. Van Dyck. Correction of non-linear thickness effects in haadf stem electron tomography. *Ultramicroscopy*, 116(0):8 – 12, 2012.

[8] K.J. Batenburg, S. Bals, J. Sijbers, C. Kübel, P.A. Midgley, J.C. Hernandez, U. Kaiser, E.R. Encina, E.A. Coronado, and G. Van Tendeloo. 3d imaging of nanomaterials by discrete tomography. *Ultramicroscopy*, 109(6):730–740, May 2009.

[9] E. Biermans, L. Molina, K.J. Batenburg, S. Bals, and G. Van Tendeloo. Measuring porosity at the nanoscale by quantitative electron tomography. *Nano Lett.*, 10(12):5014–5019, 2010.

[10] W Hoppe and R. Hegerl. *Computer processing of electron microscope images*, chapter Three-dimentional structure determination by electron microscopy. Springer-Verlag, 1980.

[11] C. Kübel, D. Niemeyer, R. Cieslinski, and S. Rozeveld. Electron tomography of nanostructured materials - towards a quantitative 3d analysis with nanometer resolution. *THERMEC 2009, Materials Science Forum*, pages 2517–2522, 2010.

[12] H. Heidari Mezerji, W. Van den Broek, and S. Bals. A practical method to determine the effective resolution in incoherent experimental electron tomography. *Ultramicroscopy*, 111(10):330–336, 2011.

[13] P.W. Hawkes. The electron microscope as a structure projector. In J. Frank, editor, *Electron Tomography, Three dimensional imaging with the transmission electron microscope*, number 2, pages 17–38. Plenum Press, 1992.

[14] Daniel Wolf, Axel Lubk, Hannes Lichte, and Heiner Friedrich. Towards automated electron holographic tomography for 3d mapping of electrostatic potentials. *Ultramicroscopy*, 110(5):390 – 399, 2010.

[15] S.J. Pennycook. Z-contrast transmission electron-microscopy - direct atomic imaging of materials. *Annual Review of Materials Science*, 22:171–195, 1992.

[16] S.J. Pennycook. Z-contrast stem for materials science. *Ultramicroscopy*, 30(1-2):58–69, 1989.

[17] P. Hartel, H. Rose, and C. Dinges. Conditions and reasons for incoherent imaging in STEM. *Ultramicroscopy*, 63:93–114, 1996.

[18] L. Reimer and H. Kohl. *Transmission Electron Microscopy: Physics of Image Formation*. Springer, 2008.

[19] N. Balakrishnan. *Handbook of Logistic Distribution*. Marcel Dekker inc., January 1992.

[20] M.N. Gibbs and D. J C MacKay. Variational gaussian process classifiers. *Neural Networks, IEEE Transactions on*, 11(6):1458–1464, 2000.

[21] H. Wang, J. Cuppens, E. Biermans, S. Bals, L. Fernandez-Ballester, K.O. Kvashnina, W. Bras, M.J. Van Bael, K. Temst, and A. Vantomme. Tuning of the size and the lattice parameter of ion-beam synthesized pb nanoparticles embedded in si. *Journal of Physics D-Applied Physics*, 45(3):–, 2012.

[22] R.H.M. Schoenmakers, R.A. Perquin, T.F. Fliervoet, W. Voorhout, and H. Schirmacher. High resolution, high throughput electron tomography reconstruction, 2005.

[23] C. Kübel. Quantitative nanoscale analysis in 3d using electron tomography. In *Proceedings of the 17th International Microscopy Congress, Rio de Janeiro, 19-24 September, 2010*, 2010.

[24] W.K. Brown and K.H. Wohletz. Derivation of the weibull distribution based on physical principles and its connection to the rosin-rammler and lognormal distributions. *J. Appl. Phys.*, 78(4):2758–2763, August 1995.

[25] T.T. Kodas and M.J. Hampden-Smith. *Aerosol Processing of Materials*. Wiley-VCH, New York, 1999.

[26] W. Van den Broek, S. Van Aert, P. Goos, and D. Van Dyck. Throughput maximization of particle radius measurements through balancing size versus current of the electron probe. *Ultramicroscopy*, 111(7):940 – 947, 2011.

Figure Captions

Figure 1. Schematic drawing of the geometry of a single tilt axis tomography experiment of a pillar-shaped specimen. The principle tomography axes are shown.

Figure 2. A schematic drawing showing the analytical model of the ESF. The intensity profile acquired from the reconstruction of the particle is modeled as a function of distance, using two combined sigmoid curves. Parameters a_1 and a_2 correspond to the intensities inside and outside the particle, respectively and the grey disk represents the particle.

Figure 3. The intensity in the center of the Pb particles as a function of particle diameter. The solid curve gives the simulation and the points the experiments.

Figure 4. The solid curve shows the relation between the real particle diameter and the diameter obtained from segmentation. The deviation from the ideal case (dashed curve) is caused by the convolution with the $\mathrm{PSF_{3D}}$ and places a lower bound of 4.4 nm on the estimation of the diameter. The solid curve is used to correct the measured diameters and is denoted as the correction function in this paper.

Figure 5. Volume rendering of the reconstructed Pb nanoparticles dispersed in Si matrix. The series is acquired over a tilt range of $\pm 90\,^{\circ}$.

Figure 6. A diagram showing how the measurements are performed. Three one-dimensional PSF are measured and then a simulated $\mathrm{PSF_{3D}}$ is calculated. The resulting $\mathrm{PSF_{3D}}$ is convolved with simulated particles of varying diameters after which the intensity at the center of the particle is measured.

Figure 7. Particle diameter distributions from a set of reconstructed Pb nanoparticles, (a) segmented using a single graylevel as a threshold and (b) after the correction scheme explained in section 4.